C. R. Chimie 21 (2018) 1270–1286

Contents lists available at ScienceDirect

Comptes Rendus Chimie

www.sciencedirect.com

Account/Revue

Surfaces, thin films and patterning of spin crossover compounds

Surfaces, croissance et structuration de films minces de composés à transition de spin

Talal Mallah [a, **], Massimiliano Cavallini [b, *]

[a] *Institut de chimie moléculaire et des matériaux d'Orsay (ICMMO), Université Paris-Sud (Paris-11), 15, rue Georges-Clemenceau, 91405 Orsay cedex, France*
[b] *Istituto per lo Studio dei Materiali Nanostrutturati (ISMN), Consiglio Nazionale delle Ricerche, Via P. Gobetti 101, 40129 Bologna, Italy*

ARTICLE INFO

Article history:
Received 27 November 2017
Accepted 12 February 2018
Available online 24 March 2018

Keywords:
Spin crossover
Films
Patterning
Nanofabrication

ABSTRACT

Spin crossover compounds are multifunctional switching materials that change their spin state and many other physical properties, such as colour, magnetic susceptibility, electric conductivity, dielectric constant and mechanical properties, upon external stimuli. Spin crossover materials have been proposed for a variety of technological applications that require the elaboration of highly controlled thin films and patterns. Here, we present a brief overview of the most diffused approaches for thin film growth and patterning, showing both conventional and unconventional approaches and the most recent advancement in their applications, highlighting the most promising cases and the most critical problems.

Mots-clés:
Transition de spin
Films
Structuration
Nanofabrication

RÉSUMÉ

Les composés à transition de spin sont des matériaux moléculaires multifonctionnels commutables. Leur état de spin ainsi que d'autres propriétés physiques comme la couleur, la conductivité électrique, la constante diélectrique, les propriétés mécaniques peuvent être modulés et contrôlés par une perturbation extérieure. Ces matériaux ont un potentiel important dans des applications comme le stockage de l'information, la thermométrie, les systèmes micro- et nano-électromécaniques, etc., qui nécessitent un contrôle fin de leur mise en forme en couches minces continues et/ou structurées. Nous présentons ici une revue brève sur les approches conduisant à la croissance de films minces et à leur structuration pour différentes applications, montrant les cas les plus prometteurs et analysant les problèmes les plus critiques.

* Corresponding author.
** Corresponding author.
E-mail addresses: talal.mallah@u-psud.fr (T. Mallah), m.cavallini@bo.ismn.cnr.it (M. Cavallini).

https://doi.org/10.1016/j.crci.2018.02.007
1631-0748/

1. Introduction

The spin crossover (SCO) phenomenon was observed for the first time in 1964 in a molecular material $Fe(phen)_2(NCS)_2$ (phen is 1,10-phenanthroline) [1] and was recognized and rationalized 2 years later due to a change in the spin state of the complex upon a change in temperature [2]. Thermodynamic considerations demonstrate that, because of entropic effects, the high-spin (HS) state is stable at high temperature, whereas the low-spin (LS) state is stable at low temperature [3]. In their first article, König and Majeda [2] showed that the change in the spin state occurs within a range of 3 K, which corresponds to an abrupt transition rather than a mere conversion (Boltzmann distribution law) between the singlet and the quintet spin states separated by an energy gap. Indeed, if one considers an assembly of noninteracting SCO molecules within the solid, a smooth change from HS to LS is expected upon decreasing the temperature [3,4]. The observation of an abrupt transition was recognized as the sign of the presence of some degree of cooperativity that, if it becomes large enough, may lead to the appearance of a thermal hysteresis loop and thus to bistability [3,4]. Although the SCO phenomenon is molecular in essence, bistability occurs if the local spin state change can be transmitted across the molecular material by elastic forces. Elastic interactions may be dominant because the change in the spin state is accompanied by a local structural change (decrease in volume when going from HS to LS) that impacts the whole material [5]. Besides the thermal spin transition, which is the most studied property in SCO, the switching process that involves a structural change produces a response that can be monitored by measuring a variety of physical properties such as colour, thermal and electric conductivity, dielectric constant and mechanical properties [6–11]. The combination of all these properties confers to SCOs an enormous potential impact in several fields of technology such as molecular memories, chemical sensors, displays [9–14] and more recently in hybrid electronics [15], spintronics and optoelectronics [16]. However, two bottlenecks for the use of SCO materials in technology and particularly in nanotechnology are the effects of size reduction and crystallinity of the nanomaterials on the degree of cooperativity and thus on bistability. Efforts to address these important issues started as early as 1988 [17], first by elaborating thin films and then nanoparticles [18–22] with two motivations: (1) to fundamentally understand the SCO phenomenon at the nanoscale when surface and environment effects become dominant and (2) for applications to integrate the nanoobjects and thin films in devices. It is worth noting that conjectures on size reduction effects were made in 1992 stating that a decrease in the grain size of an SCO material may convert an abrupt transition to a gradual conversion and favour residual HS species at low temperature [13]. For many applications, a major issue is the temperature at which the device operates in addition to improved stability and processability, which are parameters that in the past have strongly limited the technological development of SCO. Thanks to a big effort performed in chemical design and synthesis, now several families of compounds switchable around room temperature with thermal hysteresis are available [13,23–30]. They can be processed by the most diffused techniques used in research laboratory industries, such as vacuum sublimation, spin coating, drop casting, and several kinds of lithography [31]. These recent advancements have further pushed SCO towards the technological applications that require a fine control of the structure positioning and the homogeneity of thin films. This article is not aimed to be an exhaustive review of SCO films/patterns, which are discussed elsewhere [31], here, we provide a general overview, selecting the most representative examples of the recent progress made in film growth and patterning focussing on the principal growth phenomena, self-organization properties of material exploited for their fabrication.

2. Surface and thin films

In this section, we will review the work carried out on thin films and molecules on surfaces insisting mainly on the point of view of cooperativity, which is one of the main issues in the area of SCO materials that depend on size, crystallinity and organization effects. One of us have recently reviewed the different methods used to grow films of SCO materials [31].

First, it is worth mentioning briefly the main results on SCO nanoparticles related to the question of cooperativity; another article in this issue focuses in more details on this aspect. The main motivation for the elaboration of nanoparticles concerned the study of the size effect on their degree of cooperativity. These studies led to the emergence of other important aspects related to the effect of an environment enhanced by a large surface to volume ratio that is also crucial when dealing with thin films. It was shown that, keeping the same size, different switching behaviours may occur depending on the crystallinity of the objects, the state of their surface, their interaction with the surroundings and the interaction among the particles through the media holding them together [32]. Furthermore, although in many cases hysteresis tends to disappear upon decreasing the size of the objects, it may be restored below a given size [33]. The results on nanoparticles may serve to understand effects that may arise in ultrathin continuous films and patterns of such thin films.

2.1. Langmuir–Blodgett approach

The first reports on the preparation of thin films of SCO systems concerned the elaboration of a two-dimensional (2D) assembly using the Langmuir–Blodgett (LB) technique [34]. A modified version of *cis*-$Fe(phen)_2(NCS)_2$, where phen was replaced by X_2Yphen (Fig. 1) containing hydrophobic chains, allows after compression assembling the molecules at the water/air interface as monolayers [17,35,36].

The molecules forming the monolayer are oriented with aliphatic chains standing upright out of water and the polar moiety beneath the water surface, which leads to specific contacts between the molecules' cores that are different from that of the powder. The spin transition was studied on a film made of 200 monolayers transferred on CaF_2, by performing variable temperature infrared studies of the

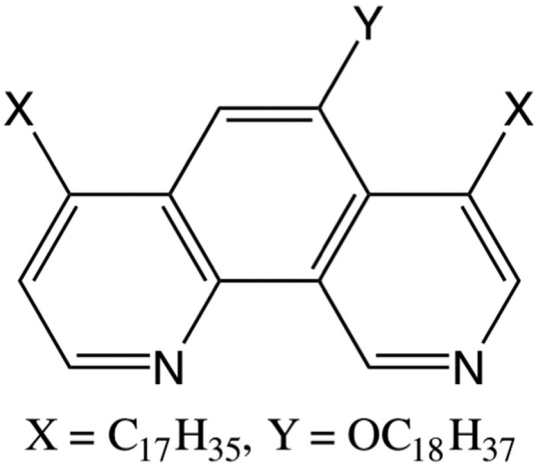

Fig. 1. Schematic view of the phen ligand modified by hydrophobic chains.

C–N vibration mode of the thiocyanate ligand in the range of 2000–2150 cm^{-1}. The study reveals the occurrence of an SCO at a temperature (T_C) equal to 263 K slightly larger than when it is in the powder form (230 K) and much larger than that for the reference compound *cis*-$Fe(phen)_2(NCS)_2$ (176 K). Moreover, the transition for the LB film was more abrupt (over a range of 75 K) than that of the powder (over a range of 200 K) revealing some degree of cooperativity, although much less than that for *cis*-$Fe(phen)_2(NCS)_2$. These results highlight two important aspects: (1) separating the SCO molecules by long chains suppresses almost completely the cooperative behaviour and (2) organizing the molecules in two dimensions restores part of the cooperative behaviour. Another observation was the presence of about 20% of residual HS species at low temperature that was thought to be due to the incorporation of some molecules of the HS precursor $Fe(pyridine)(X_2\text{-}Yphen)(NCS)_2$ within the LB film.

Operating at the water/gas interface may lead to a slight decomposition of the complexes because of the instability of the $Fe(L)_2(NCS)_2$ molecules when in contact with water [37]. Perfectly stable Langmuir films can be obtained when formamide/water mixtures are used as the subphase. When L is a modified 2,2′-bipyridine ligand containing either a long aliphatic chain or with the photoisomerizable styryl group, the fraction of HS molecules remaining at low temperature was found equal to 70%. When the LB film was annealed at 400 K, the residual HS fraction decreases to 30%. This result highlights the influence of the organization of the molecules within the film on the completeness of the spin conversion. No light effect could be observed, probably because the organization of the molecules in two dimensions precluded the isomerization of the styryl group as observed for the bulk [38]. The light-induced excited spin state trapping (LIESST) effect [39,40] was observed for the first time in an LB film made from $Fe(L')_2(NCS)_2$ (L′ is bipyridine modified by a long fluorinated chain) in 1999 [41]. A faster population of the excited state for the LB film was observed in comparison to the powder; it was correlated with the better organization of the molecules. More recently, single layers of 1D polymeric [42] and molecular [43] Fe(II) SCO systems based on the triazol ligand were elaborated by the LB technique; they present a gradual crossover close to 300 K, but without thermal hysteresis.

The studies on the LB films and the related powder lead to the conclusion that the cooperativity and completeness of the SCO is extremely sensitive to the degree of the organization of the molecules and their environment; the presence of the aliphatic chains may also alter the optical and dielectric properties of the SCO material.

2.2. Multilayers of SCO coordination networks by sequential assembly growth

The first attempt to grow films of SCO materials on a solid surface was carried out in 2006 using the sequential assembly approach of coordination networks developed by Mallouk and co-workers [44–46]. Before developing further this aspect, it is important to mention that SCO was discovered in molecular crystals that are composed of coordination complexes with only weak interactions (H-bonds, van der Waals, electrostatic, π–π stacking, etc.) among the molecules within the crystal. However, to magnify cooperativity, coordination networks with coordination bonds spreading in one, two and three dimensions were also reported as early as 1990 [23,47–50]. One interesting family is the 2D coordination networks of $[Fe(py)_2M(CN)_4]$ (M = Ni, Pd, Pt and py = pyridine) based on the Hofmann clathrate systems [51]. They are made from the assembly of Fe(II) ions by square planar $Ni(CN)_4^{2-}$ species forming a 2D square-like network with pyridine occupying the apical positions of the Fe(II) ions (Fig. 2) and present a cooperative SCO around 170 K.

Replacing pyridine by pyrazine, a bridging ligand allowed connecting the 2D layers and building 3D coordination networks with enhanced cooperativity and an increase in the spin transition temperature [24]. The structure of these systems is particularly adapted to grow thin films using a multilayer approach because the 3D network is made from 2D layers connected together by a bridging ligand in the third dimension. To elaborate films of the 3D networks, Cobo et al. functionalized a gold substrate with a mercaptopyridine layer and then constructed a robust templating film by dipping the substrate in a solution containing $Fe(BF_4)_2$ and then 4,4′-azopyridine instead of pyrazine. Dipping such film sequentially (20 cycles) in the Fe(II) and then pyrazine solutions allowed growing a

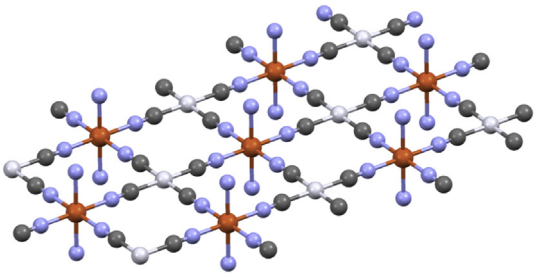

Fig. 2. View of the structure of the square-like 2D layer formed from the assembly of Fe(II) (orange) and $M(CN)_4^{2-}$; the nitrogen atoms (blue) at the Fe apical positions belong to pyridine molecules.

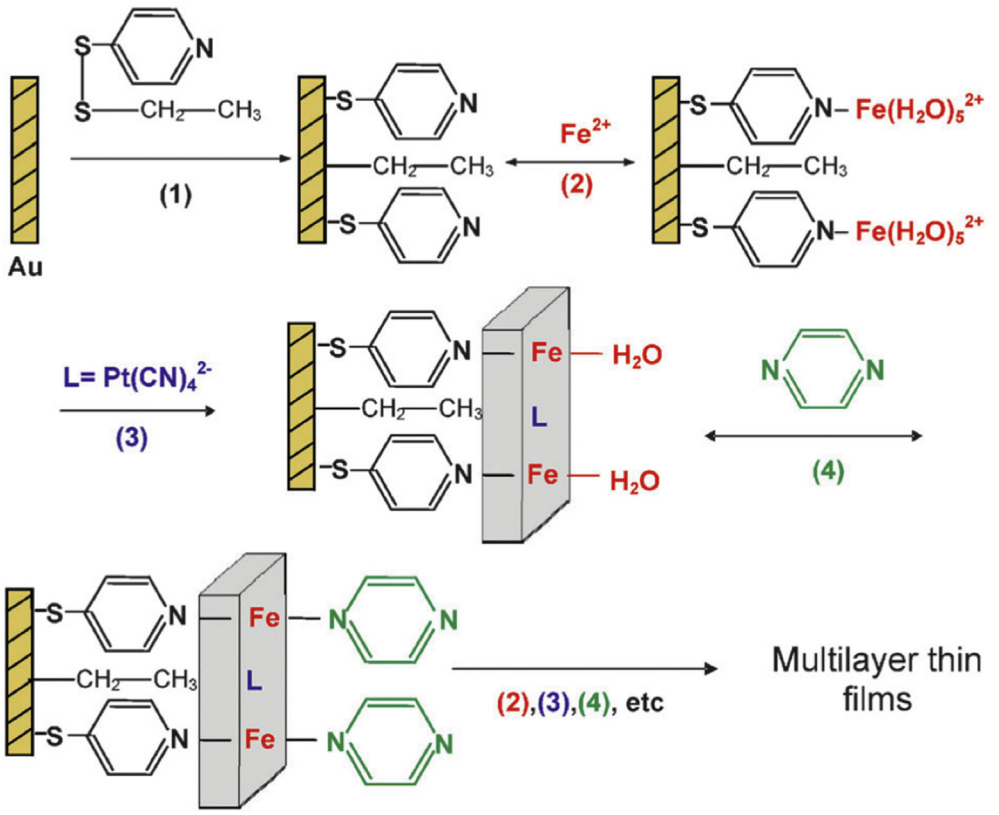

Fig. 3. Schematic procedure of the layer-by-layer growth of [Fe(pyrazine)(Pt(CN)$_4$)] multilayer thin films. Reproduced with permission from Ref. [52]. Copyright Royal Society of Chemistry.

film of the 3D network (Fig. 3) [46]. To reduce the desorption rate of the coordinated species, the reaction was carried out at −60 °C. The SCO behaviour was investigated by Raman spectroscopy by measuring, among other vibration modes, the temperature-dependent intensity of the intense pyrazine in-plane bending mode, which exhibits a shift from 645 to 675 cm^{-1} when going from the HS to the LS state.

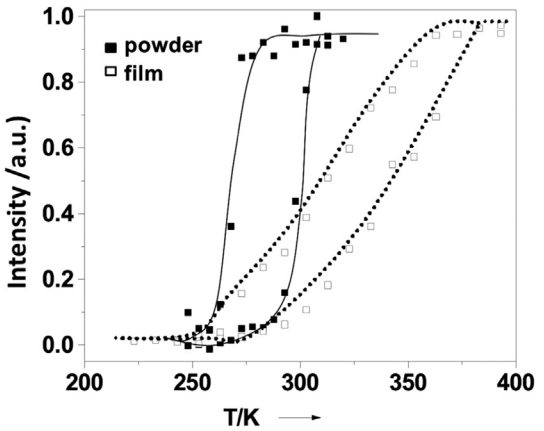

Fig. 4. Temperature dependence of the Raman intensity ratio (I (1025 cm^{-1})/I (1230 cm^{-1})) for Fe(pyrazine)[Ni(CN)$_4$] powders and films upon cooling and heating (lines are inserted to guide the eye.) Reproduced with permission from SI of Ref. [46]. Copyright Wiley-VCH.

The data collected on the film were compared with those obtained on the powder. An SCO behaviour was demonstrated for the film with a hysteresis loop almost as large as for the powder for three different samples containing M(CN)$_4$ with M = Ni, Pd and Pt [46]. Despite the presence of hysteresis for the as-prepared films, the crossover is less abrupt than for the powder, which can be due to a poor crystallinity of the films (Fig. 4). The crystallinity of the films was not investigated in this first report and no information on their thickness was given.

The thickness of the films was investigated later by atomic force microscopy (AFM) [52]; a relatively good correlation between the number of cycles and the film thickness was found, that is, a mean thickness of 3.3, 7.9 and 12.3 nm for 5, 10 and 15 deposition cycles, respectively. This is an indirect evidence for the rather good epitaxial growth of the films along the *c* crystallographic axis of the crystal (along the pyrazine bridge) where theoretical thicknesses of 3.9, 8.5 and 12.3 are calculated. Indeed, the distance between two layers obtained from X-ray diffraction on [Fe(pyrazine)(Pt(CN)$_4$]) single crystals is 7.5 Å [53]. The demonstration of the epitaxial growth of the same system using the same approach was reported later using X-ray diffraction; it showed that thin films are crystalline

and their orientations are highly controlled in both horizontal and vertical directions relative to the substrate [54]. This approach has been successfully extended to other Hofmann-like networks with 4,4′-azopyridine [55] and bis(4-pyridyl)acetylene [56] ligands. Actually, a LIESST effect was observed on the azopyridine containing films at low temperature when illuminated at 633 nm by the laser used to excite the Raman scattering.

2.3. Thin films obtained from stamping, drop casting and spin coating

Drop casting is a very useful method to elaborate thin films of molecular species, which were used many times by the SCO community and here only selected examples will be discussed. The technique relies on the introduction of long alkyl chains to obtain relatively smooth films, which unfortunately highly affects the transmission of elastic interactions over long distances and reduces the cooperativity of the materials. However, if the technique is applied on a coordination network instead of a molecular species, cooperativity and thus bistability within the network may be conserved. Kuroiwa et al. [57] reported films of the 1D coordination network based on the triazole Fe(II) compounds that possess large hysteresis around and above room temperature [13,23,49]. The approach consisted in preparing the 1D network using a triazole ligand modified by lipophilic chains that could be gelatinized in chloroform and dichloromethane and casted on highly oriented pyrolytic graphite. The SCO behaviour investigated by electronic spectroscopy shows the presence of a hysteresis loop (Fig. 5). It is important to note that bistabilty is present only in the presence of alcohols that have an optimum chain length (Fig. 5, right), highlighting the large sensitivity of cooperativity to slight chemical changes within the films.

Fe(II) complexes of Fe(4-styrylpyridine)$_4$(NCBPh$_3$)$_2$, where the styrylpyridine ligands can be in the *cis* or the *trans* isomeric forms, were prepared because the nature of the isomer leads either to HS molecules (*cis* isomer) or to SCO molecules (*trans* isomer). The SCO molecules can be transformed from the LS to the HS state by light upon transformation of the styrylpyridine ligand from the *trans* to the *cis* isomer. Efficient transformation needs the formation of transparent films containing the SCO molecules that were made by incorporating them into an acetone solution of cellulose acetate that was drop casted in a flat-bottomed glass vessel and left until complete evaporation of the solvent [58]. The high optical quality of the as-prepared films allowed investigating their SCO behaviour using electronic spectroscopy and evidenced the light-induced (322 nm) SCO from the *trans*-styrylpyridine–containing complex (LS) to the *cis*-styrylpyridine HS one at 140 K.

Recently, a large hysteresis was observed in thin films of nanoparticles deposited on graphene [59]. The films, mostly single layers, are deposited using the stamping microcontact printing technique on the single layer of the graphene device [60,61]. The thermally induced spin-state switching of the SCO nanoparticle thin films, based on the 1D system [Fe(Htrz)$_2$(trz)](BF$_4$) (Htrz = 1*H*-1,2,4-triazole), was monitored through the electrical transport properties

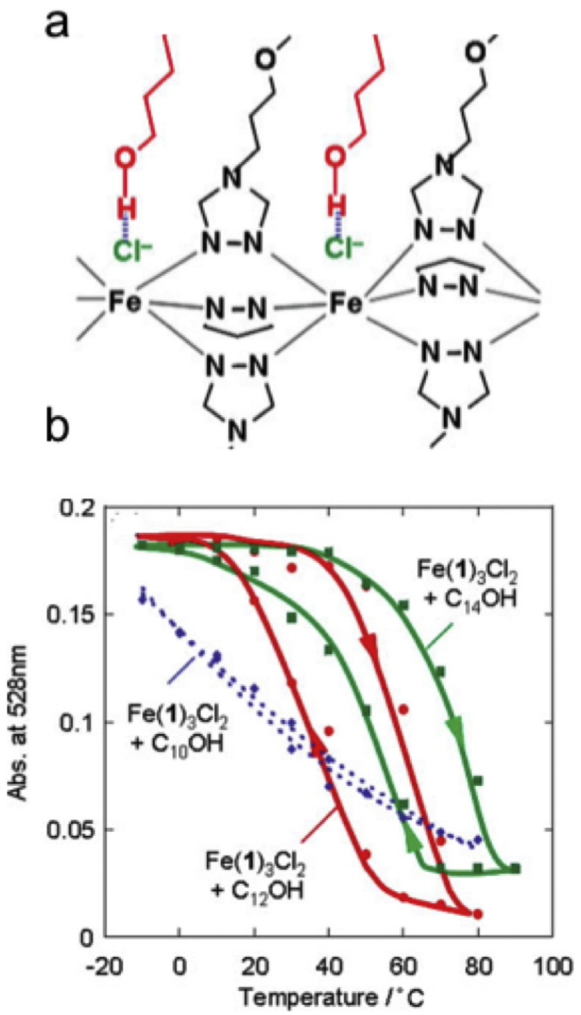

Fig. 5. (a) View of the 1D structure of the coordination network with the triazole ligand **1** modified by the lipophilic chains and (b) temperature dependence of the absorption intensity at 528 nm measured for cast films with different doping alcohols. Reproduced with permission from Figs. 6 and 7 of Ref. [57]. Copyright Wiley-VCH.

of graphene lying underneath the films. A large hysteresis cycle is observed as shown in Fig. 6. The difference with the previous cases is that here the single layer is made of rod-shaped nanoparticles (25 × 9 × 9 nm^3).

Spin coating is one of the most used methods to grow thin films with calibrated thickness: it was first used by Bousseksou et al. [62] and applied to the case of SCO materials that were studied using different techniques [63–66]. Weak cooperativity (Fig. 7) was observed in 30 nm films of [Fe(hptrz)$_3$](OTs)$_2$ (hptrz = 4-heptyl-1,2,4-triazole and OTs = tosylate) spin-coated on glass and investigated by surface plasmon resonance [67].

2.4. Films obtained from vacuum sublimation

Vacuum sublimation offers the possibility of growing films from the submonolayer to micronic thickness. The main disadvantages are the instability of the molecular

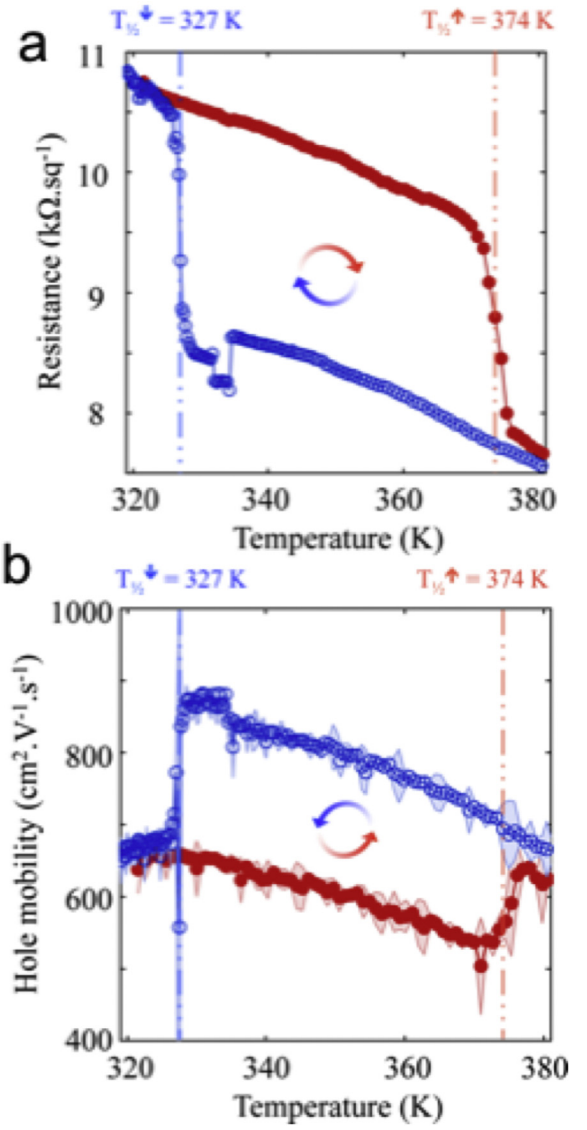

Fig. 6. Temperature dependence of graphene electrical properties after the deposition of nanoparticles. (a) Resistance per square at the Dirac point as a function of temperature for heating and cooling modes. A wide clockwise hysteresis loop is observed between 327 and 374 K. (b) Hole mobility versus temperature for the heating and cooling modes. Shaded error bars represent experimental errors in determining the field-effect mobility. Reproduced with permission from Ref. [59]. Copyright American Chemical Society.

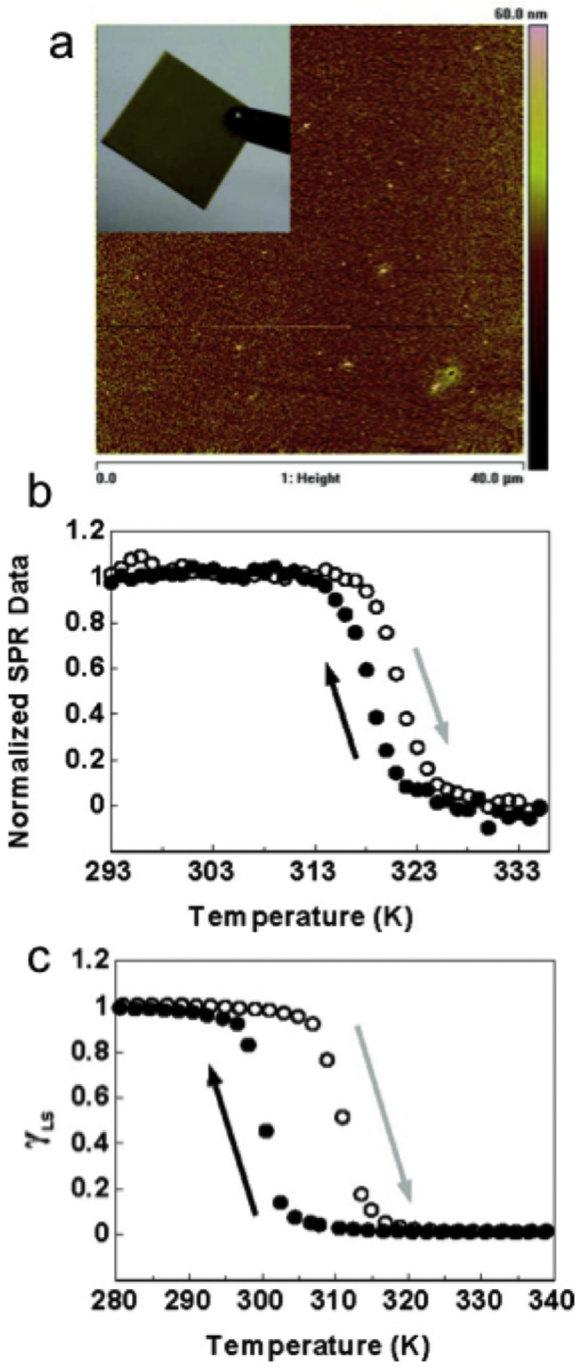

Fig. 7. (a) AFM image of a 30 nm thick $[Fe(hptrz)_3](OTs)_2$ film surface. The inset shows a photograph of the film on the glass/Ti/Au substrate and (b) temperature dependence of the plasmon resonance angle (reflectance minima) of the film in the heating and cooling modes ($dT/dt = 2$ K/min) and (c) temperature dependence of the LS fraction of the bulk complex. Reprinted with permission from Ref. [67]. Copyright American Chemical Society.

species during the sublimation process on the one hand, and on the other hand, the interaction with the substrate that may lead to the loss of part or all of the coordinated ligands. Indeed, when reactive metallic surfaces are used partial or total de-coordination of the ligands may occur if their affinity to the surface is larger than to Fe(II). This effect is enhanced due to the low concentration of the SCO molecules on the substrate if single layers are targeted [68]. Another aspect is the crystalline quality of the film. For films of thicknesses larger than few tens of nanometres, crystallites may form on the substrate and the investigated behaviour will be that of aggregated crystals rather than that of a continuous film of the material. Moreover, if smooth films are obtained with thicknesses on the order of few nanometres they are usually amorphous, which highly impacts the SCO behaviour and usually leads to the loss of

cooperativity. However, sublimation of molecular SCO species allows obtaining organized single and bilayers that can be investigated by several techniques such as scanning tunnelling microscopy (STM) and X-ray magnetic circular dichroism. The challenge is to be able to obtain organized assemblies of molecules with good crystallinity to investigate the cooperativity in two dimensions. Since the first report of the formation of films from vacuum sublimation of SCO molecules [15], an intense effort has been focused on this area.

We will first review the case of "thick films" (larger than few tens of nanometres) and then the case of single and bilayers films.

Molecules of *cis*-Fe(phen)$_2$(NCS)$_2$ were deposited under vacuum on silicon and glass substrates and lead to the formation of relatively smooth films with thicknesses ranging from 7 to 530 nm (Fig. 8) that were investigated by electronic and X-ray photoelectron spectroscopy. The magnetic behaviour investigated by SQUID shows that the 280-nm-thick film presents a SCO almost as abrupt as for the powder material demonstrating that cooperativity is kept for this thickness [15].

The second report of "thick films" focused on Fe(H$_2$B(pz))$_2$(phen) (H$_2$Bpz = bis(pyrazolyl)borate) and Fe(H$_2$B(pz))$_2$(bipy) (bipy = 2,2′-bipyridine) [69,70]. Films with thicknesses on the order of 450 nm were obtained. The films have good quality with a root mean square roughness, determined by AFM, around 3 nm. They show a SCO behaviour using UV–vis spectroscopy. The transition is less abrupt than for the powder, but it seems to still retain some cooperativity. Interestingly, the films present a LIESST effect with about 85% conversion to the HS metastable state and a T_{LIEEST} close to 50 K as in the bulk materials.

The same bis(pyrazolyl)borate-containing complexes with bipyridine and phenanthroline were investigated in the form of films made of crystallites of about 100 nm size evaporated on quartz (Fig. 9) [71].

The magnetic data of the films show a crossover from HS to LS less abrupt than for the bulk and at a slightly lower temperature; however, a very small hysteresis is present.

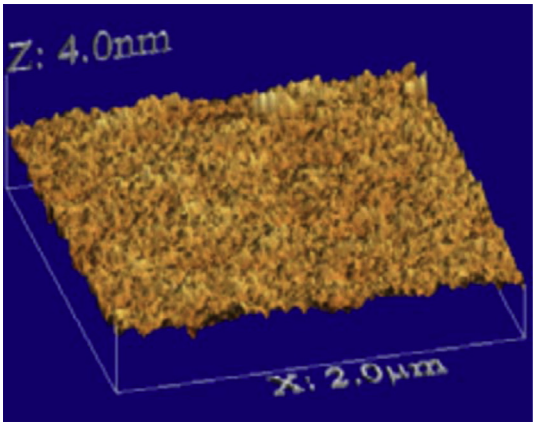

Fig. 8. AFM images of [Fe(phen)$_2$(NCS)$_2$] thin films deposited by high vacuum evaporation: (a) 280 nm on the silicon substrate (2 × 2 µm^2) and (b) 240 nm on the glass substrate (10 × 10 µm^2). Reprinted with permission from Ref. [15]. Copyright 2009© AIP.

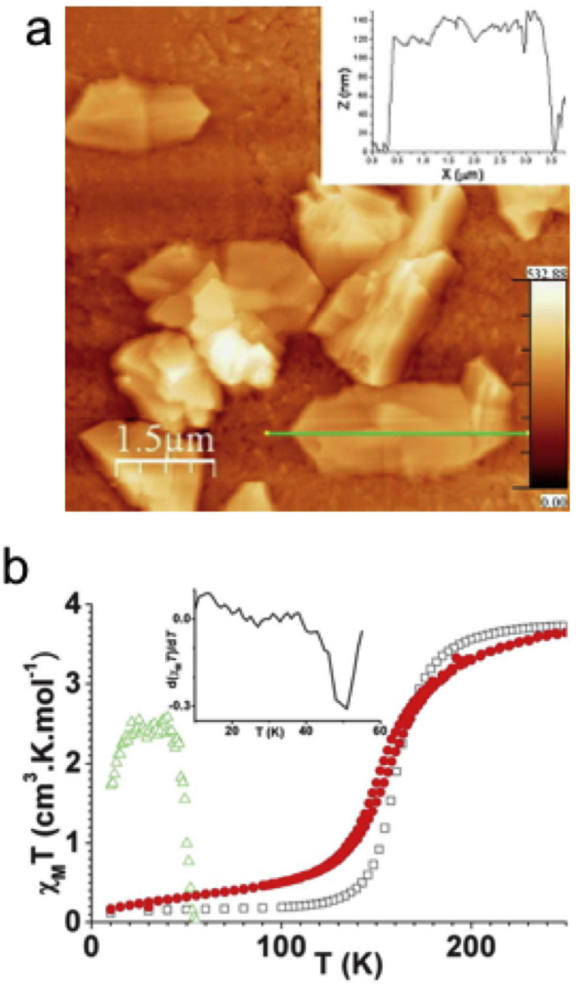

Fig. 9. (a) AFM image of [Fe(H$_2$B(pz))$_2$(bipy)] evaporated on quartz. Inset corresponds to the green line scan and (b) temperature dependence of the product χMT for [Fe(H$_2$Bpz)2(bipy)]: bulk at 1 T (black squares), thin film at 1 T over Kapton (red filled circles) and after irradiation at 5 T (green triangles). Insets: derivative d(χMT)/dT after irradiation (676 nm, 5 mW cm^{-2}). Reprinted with permission from Ref. [71]. Copyright Royal Society of Chemistry.

This behaviour is reminiscent to that observed in the case of nanoparticles of the Hofmann clathrate systems [32] and may be due to the presence of crystallites of different sizes on the substrate. The LIESST effect is also present in this case as for the smooth films mentioned above. It is also worth noting that crystallinity may have a crucial role on the abruptness of the spin transition independently of the film thickness. Indeed, the amorphous/semicrystalline films made of bipy-containing molecules have much smoother SCO than that of the more crystalline phen ones for almost any thickness.

Mastering the different parameters of the thermal vacuum sublimation allows controlling the film thickness down to few nanometres over large areas. Films of Fe(H$_2$B(pz))$_2$(phen) with 100, 30 and 10 nm thickness were obtained and integrated into a device between transparent ITO and Al electrodes [72]. The objective is to monitor the

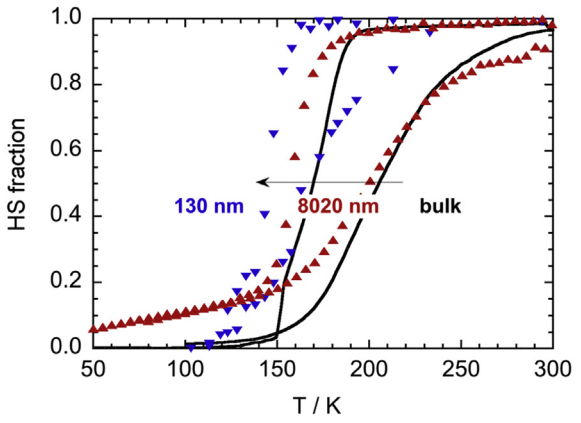

Fig. 10. SCO curve for the 130 nm (▼) and the 8020 nm (▲) thick films of [Fe($(Me_2Pyrz)_3BH)_2$] compared to the bulk (—) powder extracted from the temperature dependence of the metal-to-ligand charge transfer band relative area. Reprinted with permission from Ref. [74]. Copyright Royal Society of Chemistry.

characteristics of the device by a change in the spin state of the films (Fig. 11). Because this material presents a large LIESST effect, light was used to perform the switch from the LS state to the metastable HS state at low temperature. The device is cooled in the dark to 5 K and then irradiated through the glass and ITO by a halogen lamp. The current flow in the device drops by 7%. When the device is heated above its T_{LIESST}, the original current is recovered. This cycle can be repeated several times without loss of intensity of the light-induced change in the current.

Fe($(Me_2Pyrz)_3BH)_2$, which possesses two tridentate 2,5-dimethyl-pyrazolylborate ligands, was also sublimed and

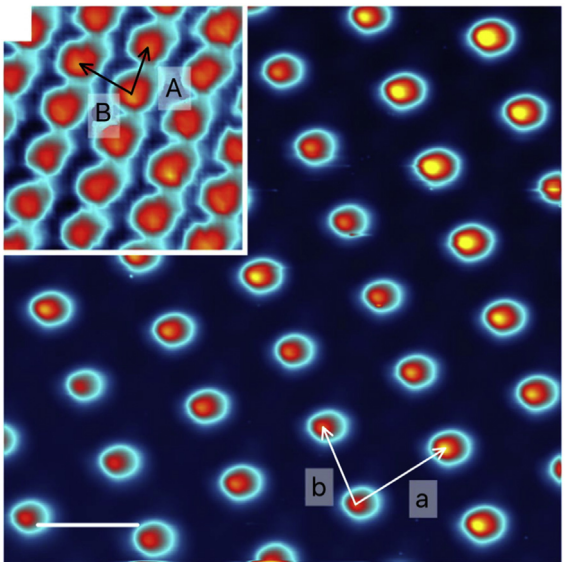

Fig. 11. STM image of [Fe($(Me_2Pyrz)_3BH)_2$] organized on a gold substrate, acquired at 0.3 V in constant height mode showing the mixed spin-state superstructure S1/3 ($\langle I \rangle$ = 50 pA). Inset: topographic STM image acquired at $V = -1.5$ V showing the full molecular crystal (I = 20 pA). The scale bar corresponds to 2 nm and is common for both images. The lattice vectors of the molecular network (A and B, black) and the S1/3 superstructure (a and b, white) are indicated. Reproduced with permission from Ref. [82]. Copyright Springer Nature.

forms thin films with different thicknesses [73,74]. In comparison with the previous compound Fe($H_2Bpz)_2$(bipy) that does not present a thermal hysteresis in the powder form, the present one has a hysteresis loop that is asymmetric with $T_{HS\rightarrow LS}$ = 174 K and $T_{LS\rightarrow HS}$ = 199 K. The 1200 nm thick film shows a wider hysteresis loop than that of the powder with the same $T_{LS\rightarrow HS}$ but with lower $T_{HS\rightarrow LS}$ = 150 K, whereas for the 570 nm film the two transition temperatures are shifted downwards and the width of the loop decreases to around 15 K [73]. The SCO was also examined by electronic spectroscopy in the UV −vis region in a less thick film (130 nm) and compared to a film that has a thickness of about 8 μm [74]. In this study, the powder was thermally sublimed under vacuum and then the films were annealed at 400 K to obtain the thermodynamically stable phase where no residual HS fraction remains at low temperature. The comparison of the HS fraction versus temperature for the two films shows that cooperativity is still present for the 130 nm film (Fig. 10), which has a root mean square roughness around 20 nm.

To study the SCO behaviour for systems that can operate around or slightly above room temperature, films of Fe($HB(tz)_3)_2$ (where tz is 1,2,4-triazol-1-yl) were elaborated with thicknesses between 20 and 200 nm. The films deposited by sublimation are amorphous. But they can be recrystallized by solvent−vapour annealing, leading to highly oriented dense crystalline films that exhibit complete and rather abrupt transition for all thicknesses, highlighting the influence of crystallinity on the thermal SCO behaviour [75]. A shift in the spin transition temperature by ca. 3 K is observed when reducing the film thickness from 200 to 45 nm, due to an anisotropy of the transformation strain in the HS phase [76]. Fe($HB(tz)_3)_2$ and its analogue Fe($HB(pz)_3)_2$ are the only evaporable SCO compounds displaying SCO above room temperature. The films with the pyrazolyl-containing compound are less crystalline and present rather gradual transition [77] in comparison to Fe($HB(tz)_3)_2$, again highlighting the importance of crystallinity on the SCO behaviour for thicknesses greater than 20 nm.

The SCO phenomenon was intensively investigated in single and bilayer films [68,78–83] after the first report of the switching performed by STM on a single molecule of Fe($phen)_2(NCS)_2$ decoupled from the gold substrate by a thin film of CuN [84]. High and low conductance states were observed for the HS and LS states, respectively. In an STM experiment, it is possible to observe a Kondo effect assigned to the HS state [85] that allows differentiating the two states [78,80]. Switching of ultrathin films was performed by visible light, vacuum-UV light [81] and also by X-rays [86] and was detected on the whole layers, which does not allow observing the switching dynamics within the film. Combining STM studies and light irradiation allowed, recently, the observation of the switching of single molecules of Fe($(Me_2Pyrz)_3BH)_2$ organized on a gold substrate [82]. The single layer film was found by STM studies, at T = 4 K, combined with theoretical calculations composed of a crystallized and ordered stable mixed phase containing one HS for two LS molecules as depicted in Fig. 11.

The response of the molecule islands was characterized after blue light illumination (405 nm). This energy

corresponds to the low-energy side of the metal-to-ligand charge-transfer absorption band that triggers the LS to HS transition by LIESST. Thus, although scanning the same area at a bias voltage of 0.3 V with an acquisition time of 5 min and 51 s per image, the sample is illuminated with an external blue diode for 10 h and then left to relax for another 10 h. During the experiment, the thermal drift in the STM images is small enough to follow the same area. Fig. 12b shows the appearance of extra atoms upon irradiation that may correspond to HS molecules. When light is switched off, only part of the molecules relaxes to the original state. The switching dynamics during illumination is complex because when, for example, a molecule switches from state 1 to state 2, a molecule within the island may convert from state 2 to state 1. Understanding the light-induced switching process of the individual molecules within the crystalline islands is one of the challenges in this area. States 1 and 2 were assigned to LS and HS, respectively. However, one must be careful because the presence of the gold surface, on which the molecules are organized, may not be innocent and may affect the light-induced process.

3. Patterning

Despite the recent progress in thin film growth, it is often difficult to grow large-scale homogeneous thin films of SCO because of the occurrence of unwanted events, such as dewetting [87], recrystallization [88], formation of polymorphs by processing [89] or because of the nature of the compound such as in the case of nanocrystals or nanoparticles. Considering that many applications need homogeneous films or nanostructures only in space-limited zones [90], patterning, that is, the growth/fabrication of SCO films or nanostructures only in controlled places of a device, represents the ideal route for fabrication. Several methods for SCO patterning have been proposed in the recent years [31], some of them based on traditional lithography, such as photolithography (PLi) and electron beam lithography (EBL) and some of them based on unconventional bottom-up methods, such as the unconventional lithography. Here, we present a brief overview of the most used methods highlighting the most recent applications. Both traditional and unconventional approaches to SCO patterning exhibit several advantages and some inconveniences, as summarized in Table 1. Traditional methods such as PLi and EBL are based on consolidated protocols and can be applied, respectively, to a large area with a few microns resolution or in a small area but with nanometric resolution (EBL). These methods take advantages from well-consolidated techniques; however, they cannot be directly used for SCO patterning because some chemical steps of the process involve aggressive chemicals that can compromise the SCO properties. Both methods were successfully used to prepare some kind of mask for successive operations with SCO compounds.

For the same reason, nanoimprint lithography (NIL), which is a consolidated nanofabrication technique capable to directly work with organic materials, combining large area fabrication with a nanometric resolution [91], is not used for direct printing of SCO films, as it needs the

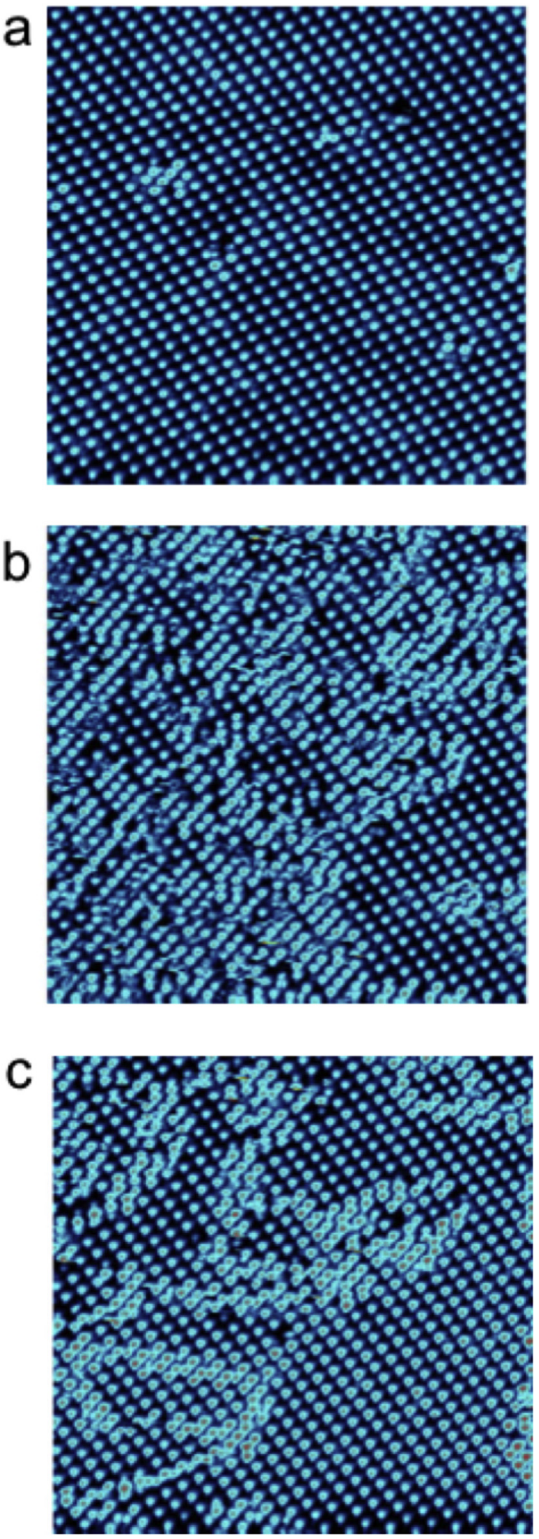

Fig. 12. STM images (4.6 K) of the same area of $[Fe((Me_2Pyrz)_3BH)_2]$ organized on a gold substrate: (a) in its initial state presenting the S1/3 superstructure, (b) under blue light illumination after 9 h and 45 min of exposure and (c) in its relaxed state 9 h and 45 min after stopping the blue light illumination ($V = 0.3$ V and $I = 20$ pA). The size of the image is 50×50 nm^2. Reproduced with permission from Ref. [73]. Copyright Wiley-VCH.

Table 1
Summary of advantages and inconveniences of nanofabrication methods used for SCO patterning.

	Method	Type	Direct application	Advantages	Disadvantages
Conventional	EBL	Serial	N	High resolution Consolidated protocols for fabrication	Small area Low throughput Cannot be directly applied to SCO film Need specific instrumentation
	PLi	Parallel	N	Large area Consolidated protocols for fabrication High throughput	Low resolution Cannot directly be applied to SCO film Need specific instrumentation
	Nanoimprinting	Parallel	N	High resolution Large area High throughput	Need a press The process can damage the SCO film
	DPN	Serial	Y	High resolution Easy to be applied	Need a special AFM Low throughput Applicable to small area
Unconventional	LCW Microtransfer moulding SAMIM Microtransfer moulding MIMIC	Parallel	Y	High resolution Versatility Rapid prototyping Large area Low cost Easy to be applied Do not need special instrumentation or special laboratory setup	Poor scalability Need soluble compounds

application of high pressure and temperature in some steps, it compromises the properties of SCO films. NIL was successfully used with SCO compounds in blend (Section 3.2) [92].

The most part of the works related to SCO patterning has been performed using unconventional wet lithography [93,94] based on soft stamps as described in Section 3.3.

All soft stamp–based methods use a soft stamp (typically polydimethylsiloxane, PDMS) for direct patterning of the SCO compounds on a substrate. When applied to SCO compounds, the soft lithographic methods show the typical advantages and inconveniences of soft lithography, such as the sustainability, low cost, simplicity (no special laboratory or setup are necessary), the multiscale control of self-organization by confinement, minimization of the amount of compound, enhancement or optimization of SCO functionalities.

All these methods start with an elastomeric polymer prepared by replica moulding of a master, which usually is fabricated by traditional lithographic methods [93]. Detailed specificity, advantages and inconveniences of each method applied to SCO are reported in successive sections.

3.1. SCO patterning by conventional lithography

PLi and EBL are consolidated approaches for micro- and nanofabrication in the electronic industry, both of them allow reproducible patterning of micro- and nanostructure on a very large area. Although they cannot be directly used for SCO patterning because some steps of the process involve aggressive chemicals that can compromise the so-fragile SCO behaviour, both methods were indirectly used for patterning of SCO by the fabrication of a mask that takes shape the zone of SCO film growth. The scheme of the processes is illustrated in Fig. 13a and b.

For both PLi and EBL the initial point is usually a flat substrate. The substrate is spin coated with an electron- or photon-sensitive resist such as polymethylmethacrylate (PMMA), which consists of macromolecules that are modified upon exposure to high-energy electrons or UV light, resulting in a transformed solubility. A desired pattern can thus be transferred to the film of resist by writing the pattern with an electron beam or by UV illumination through a mask, followed by a successive chemical development. The resulting patterned resist layer serves as a mask for successive growth of SCO thin film. Finally, a lift-off step removes the resist mask and excess material from its top, leaving the patterned structures on the substrate.

The application of traditional lithographic methods on SCO patterning was reported for the first time in 2007 by G. Molnar et al. [95] using [Fe(pyrazine)Pt(CN)$_4$] SCO and successively in different works using the same family of compounds with different ligands [52,55,56].

In particular, they report on microscale assembly of the 3D SCO coordination polymer by the fabrication of a PMMA mask followed by the growth of SCO compound by the constructive thin film growth (Fig.13c). The method is very efficient because it preserves the peculiar properties of SCO films such as the tunability of SCO properties by replacing of the different “bricks” of the film network and by the inclusions of pyridine molecules, enabling the system to be used for sensing application [52,56].

3.2. Nanoimprint lithography and dip-pen nanolithography

Recently Novio et al. [92] proposed the integration of SCO molecules in polymeric matrices as a platform for the fabrication of switchable structures exhibiting reproducible behaviour independently of the size in the range from macro- to nanoscale. SCO and PMMA are previously dissolved together in an appropriate solvent (1,2-dichlorobenzene for dip-pen nanolithography [DPN] or dichloromethane for a film for NIL) forming a

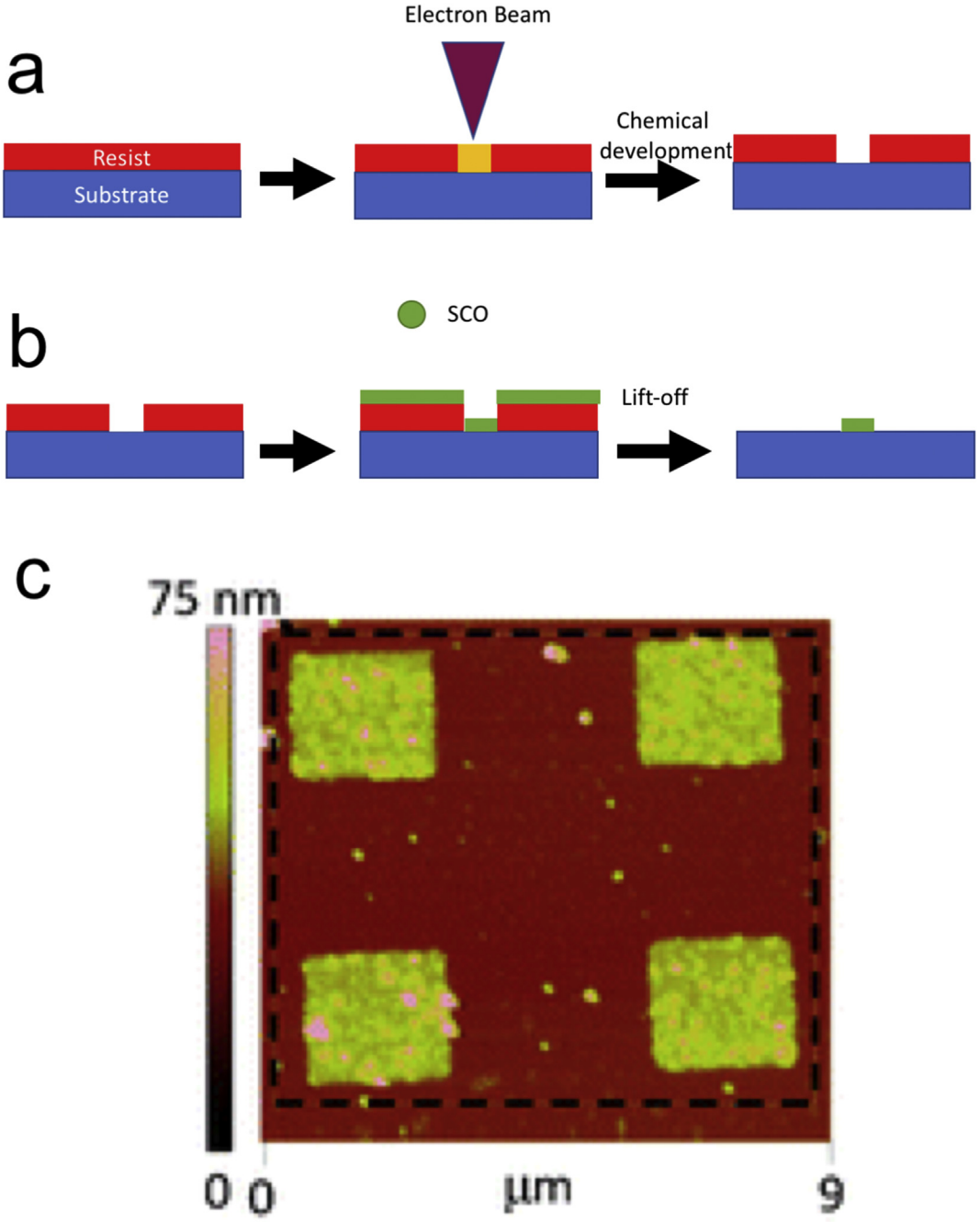

Fig. 13. Scheme of SCO patterning by EBL: (a) fabrication of polymeric mask and (b) SCO patterning. (c) AFM images of micrometric patterns of [Fe(pyrazine)$Pt(CN)_4$]. Adapted with permission from Ref. [95]. Copyright 2011 Wiley-VCH.

homogeneous solution. The proposed configuration enables the use of consolidated nanofabrication methods for polymers such as NIL and DPN. As the low percentage of SCO (<8%) contained in the mixture preserves, almost unaltered, the polymer characteristics in term of processability, the solution was directly used to pattern polymer/SCO microstructures by DPN or it was used to grow the imprintable polymeric film by spin coating.

In the case of NIL, a thin film of PMMA/SCO was spin coated on the substrate and successively imprinted using a hard stamp at a temperature higher than the glass transition temperature of the mixture. On the other hand, in the case of DPN, the 1,2-dichlorobenzene solution was directly used as printable ink by a commercial dip-pen writer. Fig. 14 shows a scheme of the processes used to pattern the PMMA/SCO microstructures and the examples of printed features.

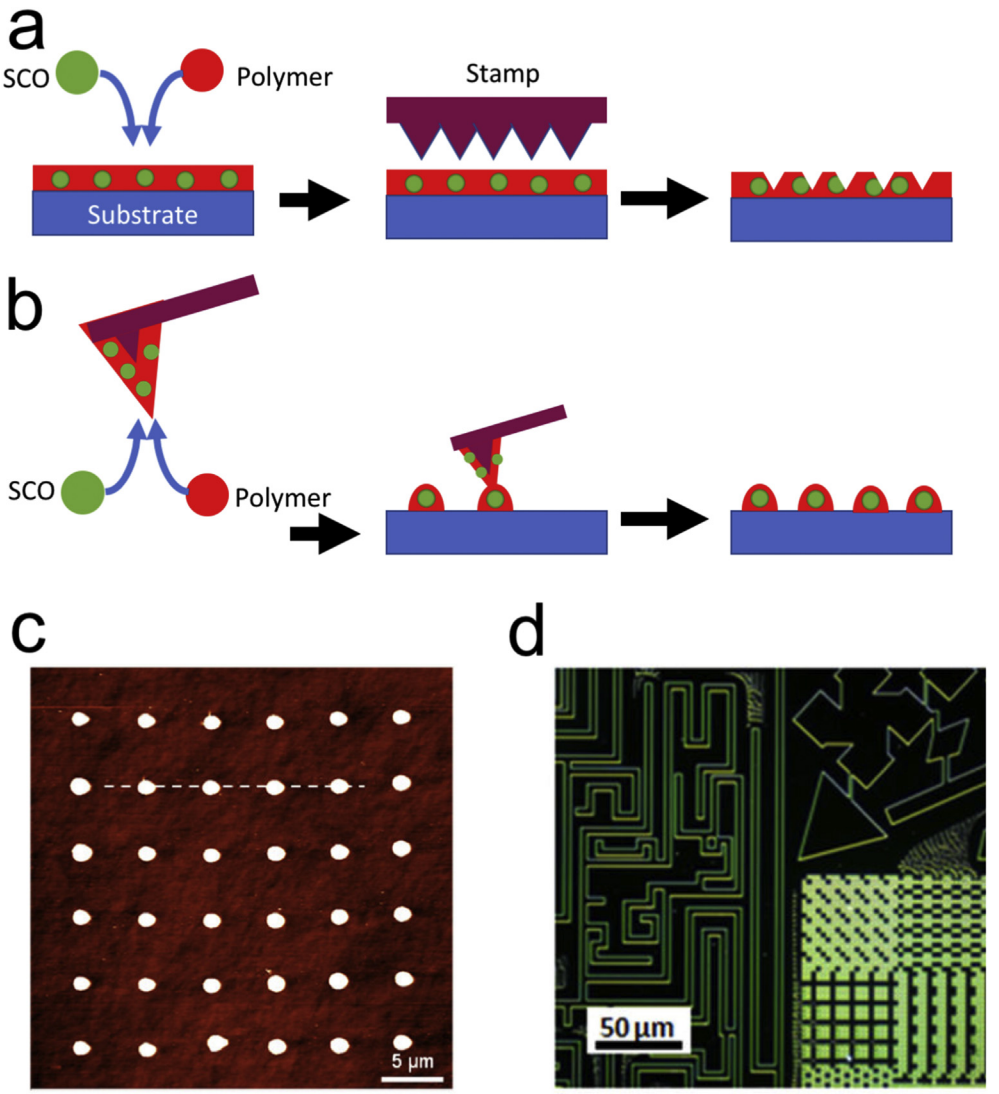

Fig. 14. (a) Scheme of NIL and (b) DPN applied to the PMMA/SCO composite. (c) AFM topography image of DPN-patterned arrays made of repeated micrometric dots. (d) Patterned structures. Panels (c) and (d) adapted with permission from Ref. [92]. Copyright Springer Nature.

3.3. SCO patterning by soft stamp lithography

The fragility of the SCO phenomenon and the poor processability of the compounds have, in the past, limited the development of SCO for many technological applications. In the last decade, this problem has been solved applying pure bottom-up wet methods that have been proven to be very efficient for the fabrication of SCO micro- and nanostructures at a controlled position; moreover, thanks to the fact that the process often involves a slow solvent evaporation, the crystallinity of micro- and nanostructures is improved [96].

The unconventional methods used to pattern SCO are based on stamp-assisted deposition in which an SCO solution is shrunk in a confined environment. This last condition results in an enhancement of long-range molecular order of deposited structures because of the reduced solvent shrinking rate during the deposition, which occurs in quasi-equilibrium conditions. Experimental results indicate that the deposition in confinement improves molecular order and in some cases, induces long-range uniaxial morphology [94,97,98].

3.3.1. Lithographically controlled wetting

In 2008, Cavallini et al. pioneered the application of unconventional bottom-up nanolithography directly using an SCO solution [12]. The approach demonstrated, for the first time, that an SCO compound could be directly patterned on several kinds of technologically relevant surfaces, preserving the SCO behaviour of the bulk material. Patterning was obtained by lithographically controlled wetting (LCW) [99], which is a versatile technique used to pattern a variety of functional materials [100,101] capable to exploit many self-organizing properties of materials, including the unwanted one such as crystallization, dewetting or thermal decomposition [102,103]. Fig. 15 shows a

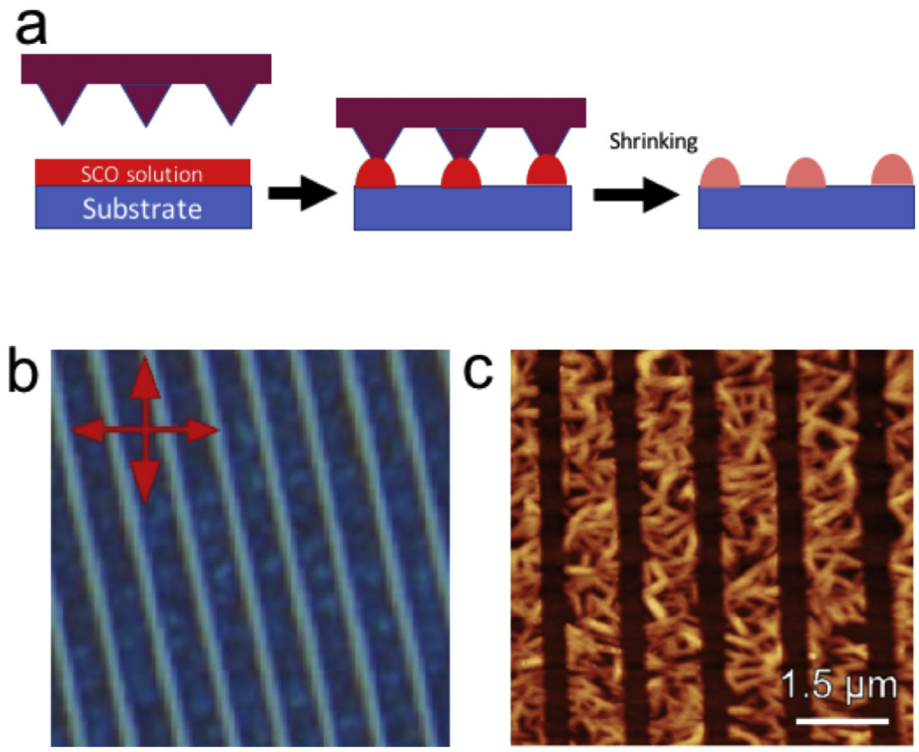

Fig. 15. (a) Scheme of LCW. (b) 10 × 10 μm^2 optical micrograph of Fe^{II}-(4′-(4‴-pyridyl)-1,2′:6′1″-bis-(pyrazolyl)pyridine)2H$(ClO_4)_3$·MeOH printed on the silicon surface. The micrograph is taken by cross-polarized optical microscopy. (c) Corresponding AFM image (*z* scale 0–80 nm). Panels (b) and (c) adapted with permission from Ref. [96]. Copyright American Chemical Society.

scheme of LCW used to pattern the Fe-(4′-(4‴-pyridyl)-1,2′:6′1″-bis-(pyrazolyl) pyridine)$_2$ microstructures and one example of printed features.

In LCW a polymeric stamp is positioned in contact with a solution film spread on a substrate. In this condition, a meniscus forms between the surface and the stamp protrusions by the capillary action. Upon shrinking, the solution remains pinned only under the protrusions leaving the regions in between them free of solution. As the solution reaches the supersaturation, the solute precipitates onto

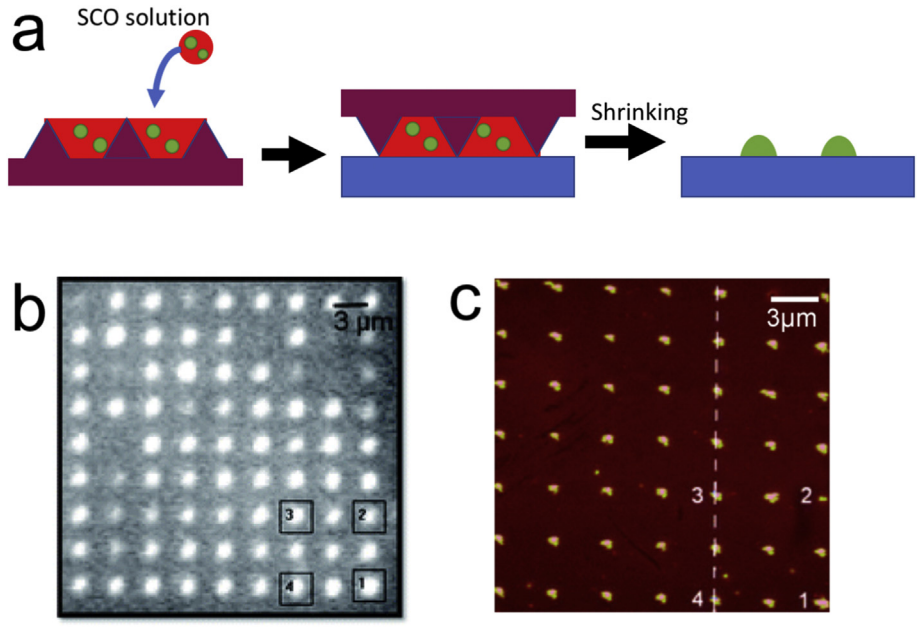

Fig. 16. (a) Scheme of the microtransfer moulding; (b) fluorescence image of printed nanodots of (and c) AFM image corresponding fluorescence image (*z* scale 0–163 nm). Adapted with permission from Ref. [110]. Copyright Royal Society of Chemistry.

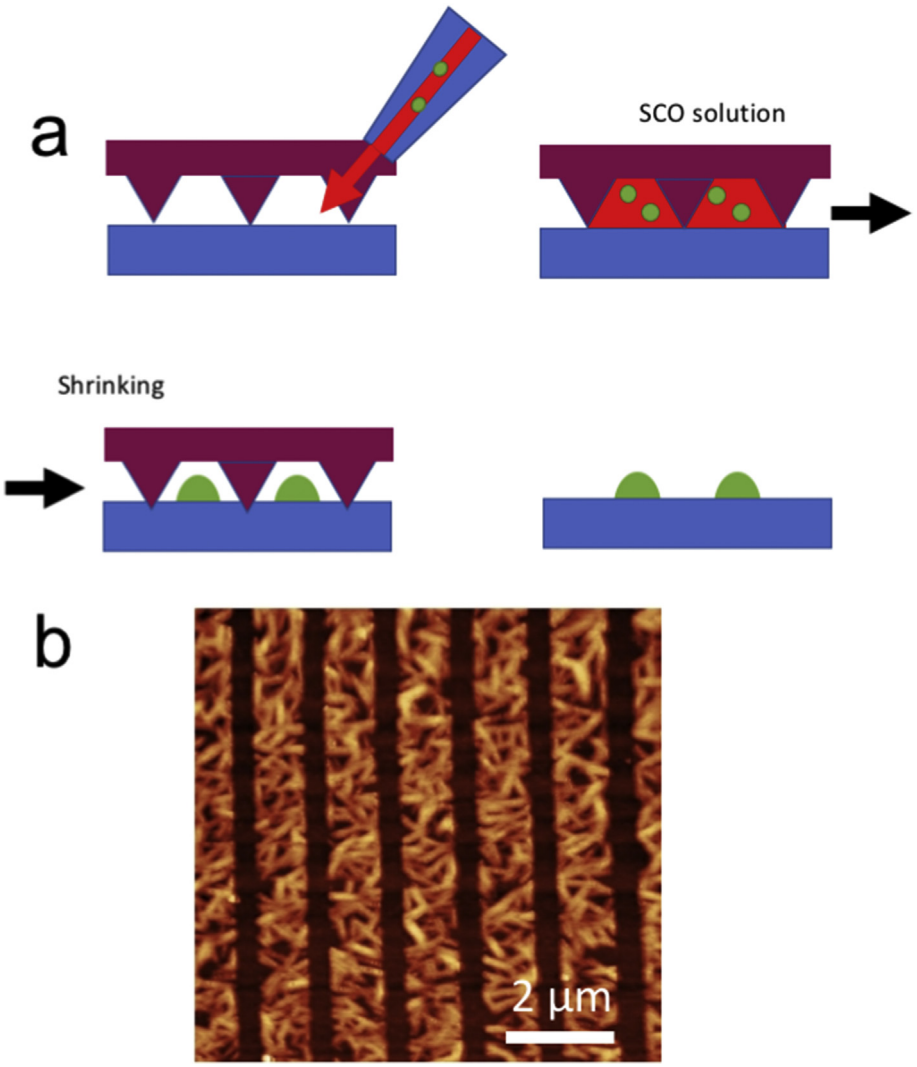

Fig. 17. a) Scheme of MIMIC. (b) AFM topography (*z* scale 50 nm) of µ-stripes of $[Fe(phen)_2(NCS)_2]$ fabricated by MIMIC on the silicon surface.

the substrate only below the protrusions, generating a pattern that replicates the stamp motif.

LCW for SCO was successfully used to pattern a variety of SCO compounds such as *cis*-$Fe(phen)_2(NCS)_2$ [12], 1D SCO compound Fe^{II}-(4′-(4‴-pyridyl)-1,2′:6′1″-bis-(pyrazolyl) pyridine)$_2H(ClO_4)_3 \cdot CH_3OH$ [96] and more recently to drive the positioning of a microcrystal at specific positions for the application of SCO in multimodal-sensing devices of a room temperature switchable $Fe(L)_2$ (LH: (2-(pyrazol-1-yl)-6-(1*H*-tetrazol-5-yl)pyridine)) [104], eventually LCW has been used to pattern a highly soluble SCO complex $[Fe^{II}$(4,4″-dioctylated 2′,6′-bispyrazolylpyrine$)_2](BF_4)_2$ embedded in a flexible and optically transparent polymer film [105].

3.3.2. Microtransfer moulding

Another efficient method used to pattern SCO compounds is the microtransfer moulding (µTM), a soft lithographic method invented in 1990s by Zhao et al. [106] for liquid precursor and successively adapted for a solution of functional materials (Fig. 16a) [107].

In µTM the solution of printable solute is deposited onto the surface of a polymeric mould (typically PDMS) removing the excess by a doctor blade. The mould is then placed in contact with a substrate and heated. After the solvent has evaporated (through the mould), the mould is carefully removed and the patterned microstructures on the substrate left. µTM is commonly used to fabricate both isolated and interconnected microstructures.

µTM was used by Thibault et al. [108] to fabricate a nanopattern of SCO nanoparticles of $[Fe(NH_2trz)](tos)_2$ over a large area.

3.3.3. Solvent-assisted micromoulding

Solvent-assisted micromoulding (SAMIM) is a soft lithographic technique conceptually similar to NIL that uses a solvent (instead of temperature) to soften the material and uses a PDMS stamp to imprint patterns into the surface of a

film. When the stamp is placed in contact with the substrate, the solvent, which is loaded in the stamp, swells a thin layer of the substrate, allowing its moulding conformal to the stamp. When the solvent evaporates, the fluid solidifies around the stamp motifs generating a pattern. Modified SAMIM were recently used to fabricate an ordered array of nanodots of $[Fe(II)(hptrz)_3](OTs)_2$ (where hptrz=4-heptyl-1,2,4-triazole and OTs = tosylate) $[Fe(II)(hptrz)_3](OTs)_2$ doped with acridine orange, reaching the spatial resolution of ~200 nm [109]. Noticeably, the luminescence intensity of the chromophore was significantly influenced by the spin transition, even in the isolated nanodots, allowing the monitoring of the SCO phenomenon by fluorescence microscopy. The same group used the modified SAMIM technique to fabricate a micrometric diffraction grating made of [110]. Noticeably, a modulation of ca. 3% on grating diffraction efficiency was observed in correspondence of the spin-state change. Fig. 16b and c show a pattern of nanodots observed by AFM and fluorescence microscopy.

3.3.4. *Micromoulding in capillaries*

Another soft lithographic method used for patterning SCO compounds is micromoulding in capillaries (MIMIC). MIMIC is considered to be the precursor of microfluidic and is applicable to pattern soluble materials [94,111]. In MIMIC, whose scheme is shown in Fig. 17a, a polymeric stamp/mould made of continuous grooves is placed onto a surface to form microchannels. As a solution is deposited at the open end of microchannels, the solution fills the microchannels by capillary action. After the complete evaporation of the solvent, which can occur also through the mould, the stamp is removed and the pattern remains on the surface. MIMIC has been efficiently proved to pattern micrometric stripes of *cis*-$Fe(phen)_2(NCS)_2$ and Fe^{II}-(4′-(4‴-pyridyl)-1,2′:6′1″-bis-(pyrazolyl) pyridine)$_2H(ClO_4)_3\cdot$MeOH compounds as shown in Fig. 17b [12,96].

4. Conclusions and perspectives

Thanks to their peculiar switching properties, SCO compounds were proposed for a variety of applications requiring the growth of films or artificially organized micro- and nanopatterns; for these reasons, the development and optimization of thin films' growth and nanopatterning methods are crucial issues. Here, we have shown how both conventional and unconventional processes for growing films of different thicknesses from several hundred of nanometres to the submonolayer and patterning were successfully used, leading to homogeneous films and ordered patterns. Many of the proved approaches are available only at a laboratory scale; however, in many cases there are no formal limitations for a possible upscaling. One of the main challenges that remain to be addressed is the growth of single layers on a large surface area with high crystallinity to assess the 2D cooperativity that is crucial for building smart devices.

Acknowledgements

This work was partially supported by National flagship NANOMAX, project N-CHEM.

References

[1] W.A. Baker, H.M. Bobonich, Inorg. Chem. 3 (1964) 1184–1188.
[2] E. Konig, K. Madeja, Chem. Commun. 3 (1966) 61–62.
[3] O. Kahn, Molecular Magnetism, VCH, 1993.
[4] O. Kahn, J.-P. Launay, Chemtronics 3 (1988) 140–151.
[5] E. Konig, Prog. Inorg. Chem. 35 (1987) 527–622.
[6] E. Breuning, M. Ruben, J.M. Lehn, F. Renz, Y. Garcia, V. Ksenofontov, P. Gutlich, E. Wegelius, K. Rissanen, Angew. Chem. Int. Ed. 39 (2000) 2504–2507.
[7] P. Gutlich, Y. Garcia, H.A. Goodwin, Chem. Soc. Rev. 29 (2000) 419–427.
[8] O. Sato, Acc. Chem. Res. 36 (2003) 692–700.
[9] S. Bonhommeau, T. Guillon, L.M.L. Daku, P. Demont, J.S. Costa, J.F. Letard, G. Molnar, A. Bousseksou, Angew. Chem. Int. Ed. 45 (2006) 1625–1629.
[10] A. Bousseksou, G. Molnar, P. Demont, J. Menegotto, J. Mater. Chem. 13 (2003) 2069–2071.
[11] F. Varret, K. Boukheddaden, E. Codjovi, A. Goujon, Hyperfine Interact. 165 (2005) 37–47.
[12] M. Cavallini, I. Bergenti, S. Milita, G. Ruani, I. Salitros, Z.R. Qu, R. Chandrasekar, M. Ruben, Angew. Chem. Int. Ed. 47 (2008) 8596–8600.
[13] O. Kahn, J. Krober, C. Jay, Adv. Mater. 4 (1992) 718–728.
[14] J. Linares, E. Codjovi, Y. Garcia, Sensors 12 (2012) 4479–4492.
[15] S. Shi, G. Schmerber, J. Arabski, J.B. Beaufrand, D.J. Kim, S. Boukari, M. Bowen, N.T. Kemp, N. Viart, G. Rogez, E. Beaurepaire, H. Aubriet, J. Petersen, C. Becker, D. Ruch, Appl. Phys. Lett. 95 (2009) 043303.
[16] M. Matsuda, H. Isozaki, H. Tajima, Chem. Lett. 37 (2008) 374–375.
[17] A. Ruaudel-Texier, A. Barraud, P. Coronel, O. Kahn, Thin Solid Films 160 (1988) 107–115.
[18] E. Coronado, J.R. Galan-Mascaros, M. Monrabal-Capilla, J. Garcia-Martinez, P. Pardo-Ibanez, Adv. Mater. 19 (2007) 1359–1361.
[19] I. Boldog, A.B. Gaspar, V. Martinez, P. Pardo-Ibanez, V. Ksenofontov, A. Bhattacharjee, P. Gutlich, J.A. Real, Angew. Chem. Int. Ed. 47 (2008) 6433–6437.
[20] T. Forestier, S. Mornet, N. Daro, T. Nishihara, S. Mouri, K. Tanaka, O. Fouche, E. Freysz, J.F. Letard, Chem. Commun. 36 (2008) 4327–4329.
[21] J. Larionova, L. Salmon, Y. Guari, A. Tokarev, K. Molvinger, G. Molnar, A. Bousseksou, Angew. Chem. Int. Ed. 47 (2008) 8236–8240.
[22] F. Volatron, L. Catala, E. Riviere, A. Gloter, O. Stephan, T. Mallah, Inorg. Chem. 47 (2008) 6584–6586.
[23] J. Krober, J.P. Audiere, R. Claude, E. Codjovi, O. Kahn, J.G. Haasnoot, F. Groliere, C. Jay, A. Bousseksou, J. Linares, F. Varret, A. Gonthiervassal, Chem. Mater. 6 (1994) 1404–1412.
[24] V. Niel, J.M. Martinez-Agudo, M.C. Munoz, A.B. Gaspar, J.A. Real, Inorg. Chem. 40 (2001) 3838–3839.
[25] S. Hayami, Z.Z. Gu, H. Yoshiki, A. Fujishima, O. Sato, J. Am. Chem. Soc. 123 (2001) 11644–11650.
[26] O. Iasco, E. Riviere, R. Guillot, M. Buron-Le Cointe, J.F. Meunier, A. Bousseksou, M.L. Boillot, Inorg. Chem. 54 (2015) 1791–1799.
[27] A.I. Vicente, A. Joseph, L.P. Ferreira, M.D. Carvalho, V.H.N. Rodrigues, M. Duttine, H.P. Diogo, M.E.M. da Piedade, M.J. Calhorda, P.N. Martinho, Chem. Sci. 7 (2016) 4251–4258.
[28] B. Weber, W. Bauer, J. Obel, Angew. Chem. Int. Ed. 47 (2008) 10098–10101.
[29] I. Salitros, N.T. Madhu, R. Boca, J. Pavlik, M. Ruben, Monatsh. Chem. 140 (2009) 695–733.
[30] S. Brooker, Chem. Soc. Rev. 44 (2015) 2880–2892.
[31] M. Cavallini, Phys. Chem. Chem. Phys. 14 (2012) 11867–11876.
[32] Y. Raza, F. Volatron, S. Moldovan, O. Ersen, V. Huc, C. Martini, F. Brisset, A. Gloter, O. Stephan, A. Bousseksou, L. Catala, T. Mallah, Chem. Commun. 47 (2011) 11501–11503.
[33] G. Felix, W. Nicolazzi, L. Salmon, G. Molnar, M. Perrier, G. Maurin, J. Larionova, J. Long, Y. Guari, A. Bousseksou, Phys. Rev. Lett. 110 (2013) 235701.
[34] On book, G.L. Gaines, Insoluble Monolayers at the Liquid Gas Interfaces, Interscience, New York, 1966.
[35] P. Coronel, A. Barraud, R. Claude, O. Kahn, A. Ruaudelteixier, J. Zarembowitch, J. Chem. Soc. Chem. Commun. 3 (1989) 193–194.
[36] P. Coronel, Etude de matériaux magnétiques en films de Langmuir-Blodgett, Thesis, Université Paris-Sud, 1990.
[37] H. Soyer, C. Mingotaud, M.L. Boillot, P. Delhaes, Thin Solid Films 327 (1998) 435–438.
[38] M.L. Boillot, H. Soyer, New J. Chem. 21 (1997) 889–892.
[39] S. Decurtins, P. Gutlich, C.P. Kohler, H. Spiering, A. Hauser, Chem. Phys. Lett. 105 (1984) 1–4.

[40] A. Hauser, J. Chem. Phys. 94 (1991) 2741–2748.
[41] J.F. Letard, O. Nguyen, H. Soyer, C. Mingotaud, P. Delhaes, O. Kahn, Inorg. Chem. 38 (1999) 3020–3021.
[42] O. Roubeau, B. Agricole, R. Clerac, S. Ravaine, J. Phys. Chem. B 108 (2004) 15110–15116.
[43] J.A. Kitchen, N.G. White, C. Gandolfi, M. Albrecht, G.N.L. Jameson, J.L. Tallon, S. Brooker, Chem. Commun. 46 (2010) 6464–6466.
[44] H. Lee, L.J. Kepley, H.G. Hong, T.E. Mallouk, J. Am. Chem. Soc. 110 (1988) 618–620.
[45] C.M. Bell, M.F. Arendt, L. Gomez, R.H. Schmehl, T.E. Mallouk, J. Am. Chem. Soc. 116 (1994) 8374–8375.
[46] S. Cobo, G. Molnar, J.A. Real, A. Bousseksou, Angew. Chem. Int. Ed. 45 (2006) 5786–5789.
[47] W. Vreugdenhil, J.H. Vandiemen, R.A.G. Degraaff, J.G. Haasnoot, J. Reedijk, A.M. Vanderkraan, O. Kahn, J. Zarembowitch, Polyhedron 9 (1990) 2971–2979.
[48] J.A. Real, E. Andres, M.C. Munoz, M. Julve, T. Granier, A. Bousseksou, F. Varret, Science 268 (1995) 265–267.
[49] O. Kahn, C.J. Martinez, Science 279 (1998) 44–48.
[50] N. Moliner, C. Munoz, S. Letard, X. Solans, N. Menendez, A. Goujon, F. Varret, J.A. Real, Inorg. Chem. 39 (2000) 5390–5393.
[51] T. Kitazawa, Y. Gomi, M. Takahashi, M. Takeda, M. Enomoto, A. Miyazaki, T. Enoki, J. Mater. Chem. 6 (1996) 119–121.
[52] C. Bartual-Murgui, L. Salmon, A. Akou, C. Thibault, G. Molnar, T. Mahfoud, Z. Sekkat, J.A. Real, A. Bousseksou, New J. Chem. 35 (2011) 2089–2094.
[53] S. Cobo, D. Ostrovskii, S. Bonhommeau, L. Vendier, G. Molnar, L. Salmon, K. Tanaka, A. Bousseksou, J. Am. Chem. Soc. 130 (2008) 9019–9024.
[54] K. Otsubo, T. Haraguchi, O. Sakata, A. Fujiwara, H. Kitagawa, J. Am. Chem. Soc. 134 (2012) 9605–9608.
[55] G. Agustí, S. Cobo, A.B. Gaspar, G. Molnár, N.O. Moussa, P.Á. Szilágyi, V. Pálfi, C. Vieu, M. Carmen Muñoz, J.A. Real, A. Bousseksou, Chem. Mater. 20 (2008) 6721–6732.
[56] C. Bartual-Murgui, A. Akou, L. Salmon, G. Molnar, C. Thibault, J.A. Real, A. Bousseksou, Small 7 (2011) 3385–3391.
[57] K. Kuroiwa, T. Shibata, S. Sasaki, M. Ohba, A. Takahara, T. Kunitake, N. Kimizuka, J. Polym. Sci. Polym. Chem. 44 (2006) 5192–5202.
[58] M.L. Boillot, C. Roux, J.P. Audiere, A. Dausse, J. Zarembowitch, Inorg. Chem. 35 (1996) 3975–3980.
[59] J. Dugay, M. Aarts, M. Gimenez-Marques, T. Kozlova, H.W. Zandbergen, E. Coronado, H.S.J. van der Zantt, Nano Lett. 17 (2017) 186–193.
[60] F. Prins, M. Monrabal-Capilla, E.A. Osorio, E. Coronado, H.S.J. van der Zant, Adv. Mater. 23 (2011) 1545–1549.
[61] J. Dugay, M. Gimenez-Marques, T. Kozlova, H.W. Zandbergen, E. Coronado, H.S.J. van der Zant, Adv. Mater. 27 (2015) 1288–1293.
[62] A. Bousseksou, P. Demont, J.F.B.I.G. Letard, L. Malaquin, J. Menegotto, L. Salmon, J.P. Tuchagues, C. Vieu, Google Patents, 2004.
[63] M. Matsuda, H. Tajima, Chem. Lett. 36 (2007) 700–701.
[64] M. Matsuda, H. Isozaki, H. Tajima, Thin Solid Films 517 (2008) 1465–1467.
[65] A. Tissot, J.F. Bardeau, E. Riviere, F. Brisset, M.L. Boillot, Dalton Trans. 39 (2010) 7806–7812.
[66] E.M. Hernandez, C.M. Quintero, O. Kraieva, C. Thibault, C. Bergaud, L. Salmon, G. Molnar, A. Bousseksou, Adv. Mater. 26 (2014) 2889–2893.
[67] G. Felix, K. Abdul-Kader, T. Mahfoud, I.A. Gural'skiy, W. Nicolazzi, L. Salmon, G. Molnar, A. Bousseksou, J. Am. Chem. Soc. 133 (2011) 15342–15345.
[68] T.G. Gopakumar, M. Bernien, H. Naggert, F. Matino, C.F. Hermanns, A. Bannwarth, S. Muhlenberend, A. Kruger, D. Kruger, F. Nickel, W. Walter, R. Berndt, W. Kuch, F. Tuczek, Chem. Eur. J. 19 (2013) 15702–15709.
[69] H. Naggert, A. Bannwarth, S. Chemnitz, T. von Hofe, E. Quandt, F. Tuczek, Dalton Trans. 40 (2011) 6364–6366.
[70] J.A. Real, M.C. Munoz, J. Faus, X. Solans, Inorg. Chem. 36 (1997) 3008–3013.
[71] T. Palamarciuc, J.C. Oberg, F. El Hallak, C.F. Hirjibehedin, M. Serri, S. Heutz, J.F. Letard, P. Rosa, J. Mater. Chem. 22 (2012) 9690–9695.
[72] C. Lefter, S. Rat, J.S. Costa, M.D. Manrique-Juarez, C.M. Quintero, L. Salmon, I. Seguy, T. Leichle, L. Nicu, P. Demont, A. Rotaru, G. Molnar, A. Bousseksou, Adv. Mater. 28 (2016) 7508–7514.
[73] V. Davesne, M. Gruber, M. Studniarek, W.H. Doh, S. Zafeiratos, L. Joly, F. Sirotti, M.G. Silly, A.B. Gaspar, J.A. Real, G. Schmerber, M. Bowen, W. Weber, S. Boukari, V. Da Costa, J. Arabski, W. Wulfhekel, E. Beaurepaire, J. Chem. Phys. 142 (2015) 194702.
[74] O. Iasco, M.L. Boillot, A. Bellec, R. Guillot, E. Riviere, S. Mazerat, S. Nowak, D. Morineau, A. Brosseau, F. Miserque, V. Repain, T. Mallah, J. Mater. Chem. C 5 (2017) 11067–11075.
[75] V. Shalabaeva, S. Rat, M.D. Manrique-Juarez, A.C. Bas, L. Vendier, L. Salmon, G. Molnar, A. Bousseksou, J. Mater. Chem. C 5 (2017) 4419–4425.
[76] V. Shalabaeva, M. Mikolasek, M.D. Manrique-Juarez, A.C. Bas, S. Rat, L. Salmon, W. Nicolazzi, G. Molnar, A. Bousseksou, J. Phys. Chem. C 121 (2017) 25617–25621.
[77] T. Mahfoud, G. Molnar, S. Cobo, L. Salmon, C. Thibault, C. Vieu, P. Demont, A. Bousseksou, Appl. Phys. Lett. 99 (2011) 053307.
[78] T.G. Gopakumar, F. Matino, H. Naggert, A. Bannwarth, F. Tuczek, R. Berndt, Angew. Chem. Int. Ed. 52 (2013) 3796.
[79] A. Pronschinske, Y.F. Chen, G.F. Lewis, D.A. Shultz, A. Calzolari, M.B. Nardelli, D.B. Dougherty, Nano Lett. 13 (2013) 1429–1434.
[80] M. Gruber, V. Davesne, M. Bowen, S. Boukari, E. Beaurepaire, W. Wulfhekel, T. Miyamachi, Phys. Rev. B 89 (2014) 195415.
[81] E. Ludwig, H. Naggert, M. Kallane, S. Rohlf, E. Kroger, A. Bannwarth, A. Quer, K. Rossnagel, L. Kipp, F. Tuczek, Angew. Chem. Int. Ed. 53 (2014) 3019–3023.
[82] K. Bairagi, O. Iasco, A. Bellec, A. Kartsev, D.Z. Li, J. Lagoute, C. Chacon, Y. Girard, S. Rousset, F. Miserque, Y.J. Dappe, A. Smogunov, C. Barreteau, M.L. Boillot, T. Mallah, V. Repain, Nat. Commun. 7 (2016) 12212.
[83] S. Ossinger, H. Naggert, L. Kipgen, T. Jasper-Toennies, A. Rai, J. Rudnik, F. Nickel, L.M. Arruda, M. Bemien, W. Kuch, R. Berndt, F. Tuczek, J. Phys. Chem. C 121 (2017) 1210–1219.
[84] T. Miyamachi, M. Gruber, V. Davesne, M. Bowen, S. Boukari, L. Joly, F. Scheurer, G. Rogez, T.K. Yamada, P. Ohresser, E. Beaurepaire, W. Wulfhekel, Nat. Commun. 3 (2012) 938.
[85] V. Meded, A. Bagrets, K. Fink, R. Chandrasekar, M. Ruben, F. Evers, A. Bernand-Mantel, J.S. Seldenthuis, A. Beukman, H.S.J. van der Zant, Phys. Rev. B 83 (2011) 245415.
[86] V. Davesne, M. Gruber, T. Miyamachi, V. Da Costa, S. Boukari, F. Scheurer, L. Joly, P. Ohresser, E. Otero, F. Choueikani, A.B. Gaspar, J.A. Real, W. Wulfhekel, M. Bowen, E. Beaurepaire, J. Chem. Phys. 139 (2013) 074708.
[87] M. Cavallini, R. Lazzaroni, R. Zamboni, F. Biscarini, D. Timpel, F. Zerbetto, G.J. Clarkson, D.A. Leigh, J. Phys. Chem. B 105 (2001) 10826–10830.
[88] M. Cavallini, M. Facchini, M. Massi, F. Biscarini, Synth. Met. 146 (2004) 283–286.
[89] D. Gentili, F. Liscio, N. Demitri, B. Schafer, F. Borgatti, P. Torelli, B. Gobaut, G. Panaccione, G. Rossi, A. Degli Esposti, M. Gazzano, S. Milita, I. Bergenti, G. Ruani, I. Salitros, M. Ruben, M. Cavallini, Dalton Trans. 45 (2016) 134–143.
[90] C. Albonetti, J. Martinez, N.S. Losilla, P. Greco, M. Cavallini, F. Borgatti, M. Montecchi, L. Pasquali, R. Garcia, F. Biscarini, Nanotechnology 19 (2008) 435303.
[91] C.C. Cedeno, J. Seekamp, A.P. Kam, T. Hoffmann, S. Zankovych, C.M.S. Torres, C. Menozzi, M. Cavallini, M. Murgia, G. Ruani, F. Biscarini, M. Behl, R. Zentel, J. Ahopelto, Microelectron. Eng. 61–62 (2002) 25–31.
[92] F. Novio, E. Evangelio, N. Vazquez-Mera, P. González-Monje, E. Bellido, S. Mendes, N. Kehagias, D. Ruiz-Molina, Sci. Rep. 3 (2013) 1708.
[93] Y. Xia, G.M. Whitesides, Angew. Chem. Int. Ed. 37 (1998) 550–575.
[94] M. Cavallini, C. Albonetti, F. Biscarini, Adv. Mater. 21 (2009) 1043–1053.
[95] G. Molnar, S. Cobo, J.A. Real, F. Carcenac, E. Daran, C. Vien, A. Bousseksou, Adv. Mater. 19 (2007) 2163–2167.
[96] M. Cavallini, I. Bergenti, S. Milita, J.C. Kengne, D. Gentili, G. Ruani, I. Salitros, V. Meded, M. Ruben, Langmuir 27 (2011) 4076–4081.
[97] D. Gentili, F. Valle, C. Albonetti, F. Liscio, M. Cavallini, Acc. Chem. Res. 47 (2014) 2692–2699.
[98] M. Cavallini, J. Mater. Chem. 19 (2009) 6085–6092.
[99] M. Cavallini, D. Gentili, P. Greco, F. Valle, F. Biscarini, Nat. Protoc. 7 (2012) 1668–1676.
[100] M. Melucci, L. Favaretto, A. Zanelli, M. Cavallini, A. Bongini, P. Maccagnani, P. Ostojo, G. Derue, R. Lazzaroni, G. Barbarella, Adv. Funct. Mater. 20 (2010) 445–452.
[101] M. Surin, P. Sonar, A.C. Grimsdale, K. Mullen, S. De Feyter, S. Habuchi, S. Sarzi, E. Braeken, A.V. Heyen, M. Van der Auweraer, F.C. De Schryver, M. Cavallini, J.F. Moulin, F. Biscarini, C. Femoni, L. Roberto, P. Leclere, J. Mater. Chem. 17 (2007) 728–735.
[102] E. Coronado, C. Marti-Gastaldo, J.R. Galan-Mascaros, M. Cavallini, J. Am. Chem. Soc. 132 (2010) 5456–5468.
[103] M. Cavallini, P. D'Angelo, V.V. Criado, D. Gentili, A. Shehu, F. Leonardi, S. Milita, F. Liscio, F. Biscarini, Adv. Mater. 23 (2011) 5091–5097.

[104] D. Gentili, N. Demitri, B. Schaefer, F. Liscio, I. Bergenti, G. Ruani, M. Ruben, M. Cavallini, J. Mater. Chem. C 3 (2015) 7836–7844.
[105] S. Basak, P. Hui, R. Chandrasekar, Chem. Mater. 25 (2013) 3408–3413.
[106] X.-M. Zhao, Y. Xia, G.M. Whitesides, Adv. Mater. 8 (1996) 837–840.
[107] M. Cavallini, M. Murgia, F. Biscarini, Nano Lett. 1 (2001) 193–195.
[108] C. Thibault, G. Molnar, L. Salmon, A. Bousseksou, C. Vieu, Langmuir 26 (2010) 1557–1560.
[109] C.M. Quintero, I.A. Gural'skiy, L. Salmon, G. Molnar, C. Bergaud, A. Bousseksou, J. Mater. Chem. 22 (2012) 3745–3751.
[110] A. Akou, I.A. Gural'skiy, L. Salmon, C. Bartual-Murgui, C. Thibault, C. Vieu, G. Molnar, A. Bousseksou, J. Mater. Chem. 22 (2012) 3752–3757.
[111] Y.N. Xia, G.M. Whitesides, Annu. Rev. Mater. Sci. 28 (1998) 153–184.